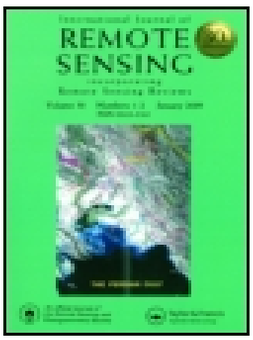

International Journal of Remote Sensing

ISSN: 0143-1161 (Print) 1366-5901 (Online) Journal homepage: https://www.tandfonline.com/loi/tres20

Evaluation of gap-filling methods for Landsat 7 ETM+ SLC-off image for LULC classification in a heterogeneous landscape of West Africa

Yaw Mensah Asare, Eric Kwabena Forkuo, Gerald Forkuor & Michael Thiel

To cite this article: Yaw Mensah Asare, Eric Kwabena Forkuo, Gerald Forkuor & Michael Thiel (2019): Evaluation of gap-filling methods for Landsat 7 ETM+ SLC-off image for LULC classification in a heterogeneous landscape of West Africa, International Journal of Remote Sensing, DOI: 10.1080/01431161.2019.1693076

To link to this article: https://doi.org/10.1080/01431161.2019.1693076

Published online: 21 Nov 2019.

INTERNATIONAL JOURNAL OF REMOTE SENSING
https://doi.org/10.1080/01431161.2019.1693076

Taylor & Francis
Taylor & Francis Group

Evaluation of gap-filling methods for Landsat 7 ETM+ SLC-off image for LULC classification in a heterogeneous landscape of West Africa

Yaw Mensah Asare[a,b], Eric Kwabena Forkuo[b], Gerald Forkuor[c] and Michael Thiel[d]

[a]WASCAL Graduate Research Programme on Climate Change and Land Use, Department of Civil Engineering, Kwame Nkrumah University of Science and Technology, Kumasi, Ghana; [b]Department of Geomatic Engineering, Kwame Nkrumah University of Science and Technology, Kumasi, Ghana; [c]West African Science Service Centre on Climate Change and Adapted Land Use, Ouagadougou, Burkina Faso; [d]Department of Remote Sensing, Institute of Geography and Geology, University of Würzburg, Würzburg, Germany

ABSTRACT

The Landsat mission which has existed over five decades has remained at the forefront of providing consistent moderate spatial and temporal resolution optical images of the earth. The failure of the scan line corrector (SLC) on board the Landsat 7 Enhanced Thematic Mapper Plus (ETM+) in May 2003 has permanently resulted in data gaps on each Landsat 7 scene. Due to the obvious negative impacts on the image usability, a number of methods have been developed to fill the no-data areas in the image. This study assessed the performance of four Landsat 7 ETM+ SLC-off gap-filling methods in a highly heterogeneous landscape of West Africa for two different seasons (dry and rainy). The methods considered are: (1) Weighted Linear Regression (WLR) integrated with Laplacian Prior Regularization Method (LPRM), (2) Localised Linear Histogram Matching (LLHM), (3) Neighbourhood Similar Pixel Interpolator (NSPI) and (4) Geostatistical Neighbourhood Similar Pixel Interpolator (GNSPI). All the images used were Landsat 7 ETM+ SLC-off images, temporally close and from the same season for each set of time step. Visual comparison, mean, and standard deviations of the histograms of all bands of only the filled areas were used to assess the results. Additionally, overall accuracy (OA), kappa coefficient (κ), and balanced accuracy (BA) per class were used to evaluate a land use/cover (LULC) classification based on the gap-filled images. Visually, all the four methods were able to completely fill the gaps in the Landsat 7 ETM+ SLC-off image. They all look similar and spatially continuous with no anomalies or artefacts on them. The histograms from each band for only the filled areas for all the four methods also gave similar means and standard deviations in most cases. All the four gap-filling methods provided satisfactory results (OA >96% and κ> 0.937 in all methods for images in the dry season and OA >93% and κ> 0.877 for the image in the rainy season) in the land cover classification considering the complexity of the study area. But the GNSPI was superiority in all cases with the highest

ARTICLE HISTORY
Received 13 November 2018
Accepted 2 September 2019

CONTACT Yaw Mensah Asare mensah.yasare@gmail.com WASCAL Graduate Research Programme on Climate Change and Land Use, Department of Civil Engineering, Kwame Nkrumah University of Science and Technology, Kumasi, Ghana

OA of 97.1% and κ of 0.947 in the dry season and OA of 94.6% and κ of 0.899 in the rainy season. This implies that the GNSPI is more robust in gap filling of Landsat 7 ETM+ SLC-off images than the other three methods in a heterogeneous landscape of West Africa regardless of the season. This study suggests that gap filling of Landsat 7 ETM+ SLC-off images will help to increase the number of Landsat images needed to build time-series data for a data-scarce region such as West Africa.

1. Introduction

Land use/cover (LULC) mapping and monitoring with optical images have been extensively used in land surface studies and applications (Ghansah et al. 2016; Jarman, Jarman, and Edwards 1983; Lunetta et al. 2006; Nyamugama and Kakembo 2015; Vittek et al. 2014; Forkuor et al. 2017a) because of its ability to produce consistent and comprehensive data in time and space . The Landsat mission, which has been operational since 1972 (Loveland and Dwyer 2012; Williams, Goward, and Arvidson 2006), has produced the most comprehensive and complete set of medium resolution optical images of the earth. It has been utilized in diverse fields of land surface research including agriculture (Hamuda et al. 2018; Leslie, Serbina, and Miller 2017), soil (Aksoy, Özsoy, and Dirim 2009; Azabdaftari and Sunar 2016; Nawar et al. 2014), water (Laili et al. 2015; Hellweger et al. 2004), forestry (White et al. 2017; Onojeghuo and Onojeghuo 2015) and settlements (Hu et al. 2016; Esch et al. 2009; Bhatti and Kumar Tripathi 2014). However, as an optical system, data availability is often hindered by persistent cloud and cloud shadow cover, making it difficult to obtain consistent data for LULC classification and trend analysis especially in tropical regions such as West Africa (WA) (Wijedasa et al. 2012). The failure of the scan line corrector (SLC) on board the Landsat 7 Enhanced Thematic Mapper plus (ETM+) instrument in May 2003 introduced a further limitation on obtaining usable and consistent data for studying LULC dynamics (Zhang, Li, and Travis 2007; USGS 2013). The function of the SLC was to compensate for the forward motion of the satellite during data acquisition. This failure has resulted in images with wedge-shaped gaps (so-called SLC-off images) that range from a single pixel near the centre of the image to about 14 pixels along the east and west edges of each scene acquired (Maxwell, Schmidt, and Storey 2007; Maxwell 2004). On average, each scene losses about 22% of the image data. Nonetheless, the remaining spectral information on such SLC-off images exhibits the same radiometric and geometric qualities as images taken before the failure (Storey et al. 2005).

Due to the obvious negative impacts of this failure on image usability, a team of scientists put together by the USGS (United States Geological Survey) was tasked to evaluate the utility and validity of Landsat 7 ETM+ SLC-off products. They noted that for applications covering large spatial scales (such as LULC changes) the impact of the anomaly was acceptable. However, for local-scale applications, the effect of the SLC-off induced data gaps may have a substantial influence on the results of the specific application under consideration (USGS 2013). Consequently, several methods have been developed to fill the gaps caused by the malfunctioning of the SLC to ensure image usability for various applications as well as to maintain the continuity of the Landsat data archive (Wulder et al. 2008).

Examples of methods developed include: (1) Linear Histogram Matching (localized and adaptive window linear histogram matching (LLHM and AWLHM)) (Scaramuzza, Micijevic, and Chander 2004), (2) Neighbourhood Similar Pixel Interpolator (NSPI) (Chen et al. 2011), (3) Geostatistical Neighbourhood Similar Pixel Interpolator (GNSPI) (Zhu, Liu, and Chen 2012), (4) Kriging (Zhang, Li, and Travis 2007), (5) Weighted Linear Regression (WLR) and Laplacian Prior Regularization Method (LPRM) (Zeng, Shen, and Zhang 2013), and the (6) Geographically Weighted Regression (GWR) method (Zhang, Li, and Civco 2014). Common to these methods is the use of other Landsat scenes (known as input images) to fill the gaps in the SLC-off images. Since the location of the gaps differs for each SLC-off scene (Storey et al. 2005), it is possible to use SLC-off images as input images. There are, however, differences in the approach each method adopts in filling the missing data pixels. For example, the number of input images required, type and number of input parameters and method used to transform input parameters for gap filling (e.g. regression, geostatistical). Yin et al. (2017) provide a good summary of most of these methods.

These differences have necessitated a number of studies which aimed at ascertaining the accuracy and suitability of the different methods in filling the missing data pixels in Landsat 7 ETM+ SLC-off images. These studies tested the methods in different landscapes in varying parts of the world. Romero-sanchez et al. (2015), for example, compared four gap-filling methods (LLHM, NSPI, GNSPI and WLR) to determine the most robust in filling SLC-off images for mapping a semi-deciduous tropical forest in Mexico. They created artificial gaps on an SLC-on, filled the gaps with the methods, and compared the gap-filled predicted pixels with the corresponding pixels in the original image. Based on accuracy measures such as overall accuracy (OA), kappa coefficient (κ), etc., they concluded that the GNSPI method performed better than the other methods (Romero-sanchez et al. 2015). In a similar research, Yin et al. (2017) applied four gap-filling algorithms – Kriging and co-Kriging, GNSPI, WLR and the DS – across a range of land surface conditions (homogeneous and heterogeneous) in scenes with abrupt changes in landscape elements. Their results showed a satisfactory performance for all of the gap-filling approaches for the homogeneous case. However, in a heterogeneous environment, GNSPI achieved the best performance for all tested cases. They found the WLR and the GNSPI methods to exhibit equivalent accuracies when temporally close images are used. For the case of abrupt changes in scene elements or in the absence of ancillary data, the DS approach performed better than the other tested methods. Following from these results, other studies have underscored the influence of landscape characteristics (homogeneity or heterogeneity) on the performance of gap-filling algorithms (Zhu, Liu, and Chen 2012; Yin, Mariethoz, and McCabe 2016; Yin et al. 2017).

Studies conducted in several parts of West Africa have alluded to rapid changes in LULC in the sub-region (Kleemann et al. 2017; Obahoundje et al. 2018). To ensure sustainable land management in the future and reduce the looming effects of climate change in West Africa, a good understanding of present and historical LULC patterns is required, which could help in predicting future patterns. Landsat images are an important data source for LULC mapping globally, but especially in data-poor regions such as West Africa. Although new high to moderate resolution open-access images are now available (e.g. the Sentinels through the Copernicus program), which could help in determining present LULC patterns, Landsat ETM+ SLC-off presents one of the most comprehensive open-access historical remote sensing data for LULC and other analysis. In this regard, investigating which of the several gap-filling algorithms works well for the heterogeneous

West African landscape is important for deriving and understanding historical LULC patterns. Further, knowledge of the best gap-filling algorithm will increase the number of available Landsat data time-series for deriving and understanding present-day LULC patterns (considering that Landsat 7 and 8 are running concurrently). This will also reduce the effects of persistent cloud cover on availability of cloud-free images. Unfortunately, not much research has been conducted in West Africa concerning the best gap-filling algorithm for the peculiar landscape of this region (Laurin et al. 2012). This submission aims at contributing to this research gap by comparing the performance of four gap-filling algorithms – WLR-LPRM, LLHM, NSPI, and GNSPI Landsat 7 ETM+ SLC-off images. These methods were selected because they are open source, user-friendly and often used methods for gap filling (Yin et al. 2017; Sadiq et al. 2014; Romero-sanchez et al. 2015). The study was conducted in South-Western Burkina Faso, which has a landscape characteristic typical of West Africa. Experiments were performed on two data time steps representing the two main seasons (dry and rainy) in the study area. The resulting gap-filled images were assessed qualitatively using the mean and standard deviations of the pixel values of the filled areas. For a quantitative assessment, the gap-filled images were classified to reveal LULC classes, and subsequently validated to produce error matrices. The balanced accuracy per class, OA and κ obtained from the error matrices were compared to judge which of the algorithms is more robust in filling the gaps of Landsat 7 ETM+ SLC-off images of heterogeneous landscapes in WA.

2. Materials and method

2.1. Study area

The experimental area is located in the South-West Region of Burkina Faso (Figure 1). It is located between latitudes 11°45′and 11°10′N and longitudes 003°10′and 003°00′W with a total area of about 1,429.73 km^2. Rainfall pattern in the area is uni-modal and starts from May to October followed by a dry season from November to April. The annual rainfall average is about 850 mm and daily temperature ranges between 20°C and 34°C (Forkuor et al. 2017b; Liu et al. 2015). The study region falls within the Sudanian savannah climatic zone with natural vegetation made up of forest, savannah woodland, grass and shrub. The major land use is agriculture. Sorghum, millet, maize, cowpea, groundnut are the main staple crops while cotton is the most important cash crop (Hipt et al. 2017). There are several rural settlements scattered within the farming areas and few major towns (which includes Dano and Diebougou) in the study area. In terms of surface water, the area has several irrigation dams and network of rivers. Illegal small-scale gold mining is gradually springing up in the area and due to its lucrative nature, people are migrating from other areas of the country into the region. Topographically, the area is relatively flat with some few hilly areas. The elevation ranges between 236 and 568 m above mean sea level. The soil types are Lixisols (most dominant), plinthosols, gleysols, cambisols, leptosols, and stagnosols (Hipt et al. 2017; IUSS 2006; Callo-Concha, Gaiser, and Ewert 2012).

2.2. Data and pre-processing

Cloud-free Landsat 7 ETM+ SLC-off images (C1-Level) of path 196 and row 052 were used in this study. The study area falls within the section of the scene where missing pixels per

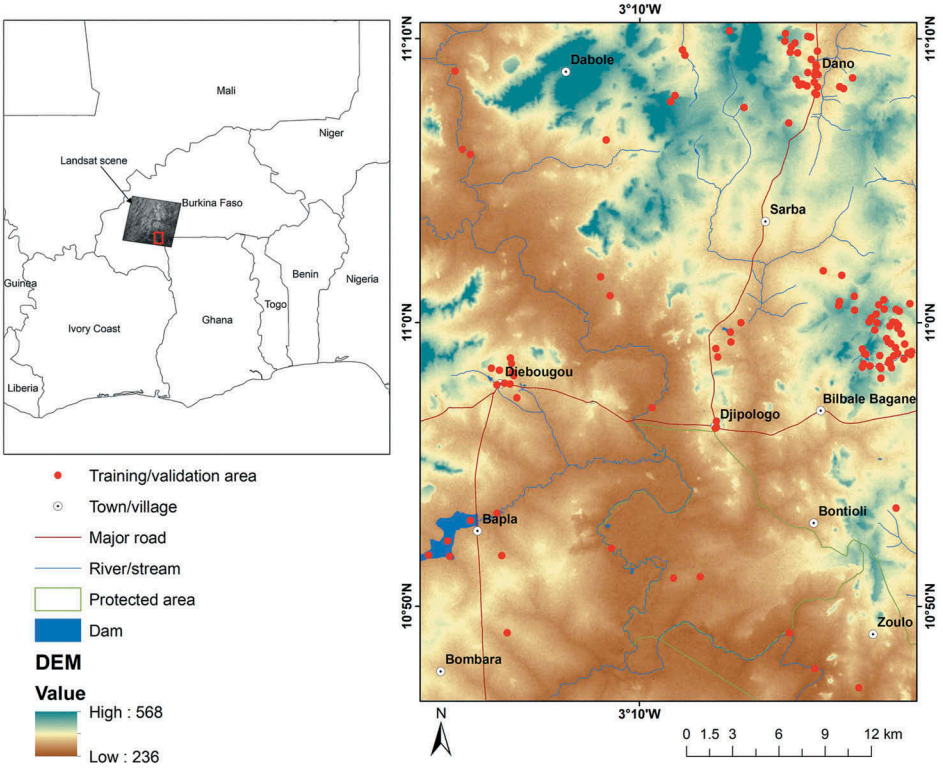

Figure 1. Map of the study area in the South-west region of Burkina Faso.

strip range from 4 to 9. Compared to the gaps at the edges of the scene (up to 14 pixels), these gaps are relatively narrow. But the accurately filling of these narrow gaps are important for understanding local-scale dynamics, which was the purpose of this study. Moreover, for subsequent classification of the gap-filled images, authors conducted field-work in the study area only. Table 1 details the images used as target and input. 'Target image' represents the image with gaps to be filled, 'input image' is the image to be used to fill the gaps in the target image. The images were selected for two different time steps. The first time-step (season 1 – S1) was taken from the dry season in the month of January in a 16 days interval between the target image and the input image. The second time step (S2) was taken from the rainy season in the months of May and June for the target and input images, respectively, and with a 16-day interval.

Our choice of image dates was influenced by cloud cover and the different seasons in the study area. The digital numbers of all images were converted to top-of-atmosphere

Table 1. Landsat 7 ETM+ SLC-off images used in the study. S1 represent images chosen from the dry season and S2 is images from the rainy season.

Time step	Purpose	Date acquired	Landsat scene ID
S1	Target image	3 January 2010	**LE71960522010003ASN00**
	Input image	19 January 2010	**LE71960522010019EDC00**
S2	Target image	25 May 2015	**LE71960522015145ASN00**
	Input image	10 June 2015	**LE71960522015161ASN00**

(TOA) reflectance using the relevant information in their respective metadata files. Atmospheric correction was not performed due to information provided by developers of some of the algorithms. For example, Chen et al. (2011) explained that the NSPI can be applied to either TOA radiance or reflectance, so far as the calibration formula is the same between input and target images. Zhu, Liu, and Chen (2012) also utilized TOA images in testing and presenting the GNSPI algorithm. Due to the gentle relief of the study area, topographic correction, as was recommended for mountainous areas by Zhu, Liu, and Chen (2012) was not performed for images.

All the six reflective bands (blue, green, red, Near-infrared (NIR), Short-wave infrared (SWIR) 1 and 2) were used in the gap-filling process. Figure 2 shows the images used in a false colour composite (band combination 4-3-2). The gap-filled images, based on the different algorithms under review, were classified to reveal five land use/land cover classes with reference to the Food and Agriculture Organization (FAO) LULC classification scheme (FAO 2000). These are vegetation, bare land, water, settlement and cropland. For training the classifiers and validating the LULC classification results, polygons of the various land-use classes were delineated using homogeneous purposive sampling approach. The training samples were obtained from high resolution (50 cm) digital globe images of 2010 and 2015 on Google Earth engine's historical images, existing topographic maps, previous LULC maps (Zoungrana et al. 2015), field visits and interviews conducted from March to December 2017. In all 123 polygons of sizes between 178 m^2 and 3328 m^2 were used.

2.3. Gap-filling methods

2.3.1. Weighted linear regression integrated with laplacian prior regularization

This approach fills image gaps by using two methods (WLR and LPRM), either separately or combined. The WLR method (Zeng, Shen, and Zhang 2013) fills the missing data pixels in the target image with an input image information by building a regression model between the corresponding pixels assuming a linear relationship between the two images covering the same area. When the target image cannot completely recover the missing pixels, a non-reference regularization algorithm is used to implement the pixel filling. In this algorithm, similar pixels of the input image will be searched, and a weighted linear regression will be built based on it. This means, the most important parameter in this process is the number of similar pixels. When the gap widths are large, the WLR method may not be able to fill all missing pixels; in that case, the LPRM method is adopted to fill the remaining gap pixels. The LPRM algorithm is a non-reference recovery method. In this process, the invalid pixels are recovered by the iterations and updates under a priori constraint. Two important parameters must be considered, the regularization parameter and the maximum number of iterations. The regularization parameter balances the data fidelity and the image regularization. The larger the parameter, the smoother the results. The maximum number of iterations determines the magnitude of the algorithm. When the invalid region is large, this parameter should increase. Otherwise, not every invalid pixel can be filled. The detailed concept of WLR-LPRM gap-filling method can be found in Zeng, Shen, and Zhang (2013) and the packaged software is available online (Shen 2014) for free. The following parameters were used in-line with the guidance from Zeng, Shen, and Zhang (2013): the number of similar pixels is 30, the regularization parameter is 1000, and the maximum number of iteration is 600.

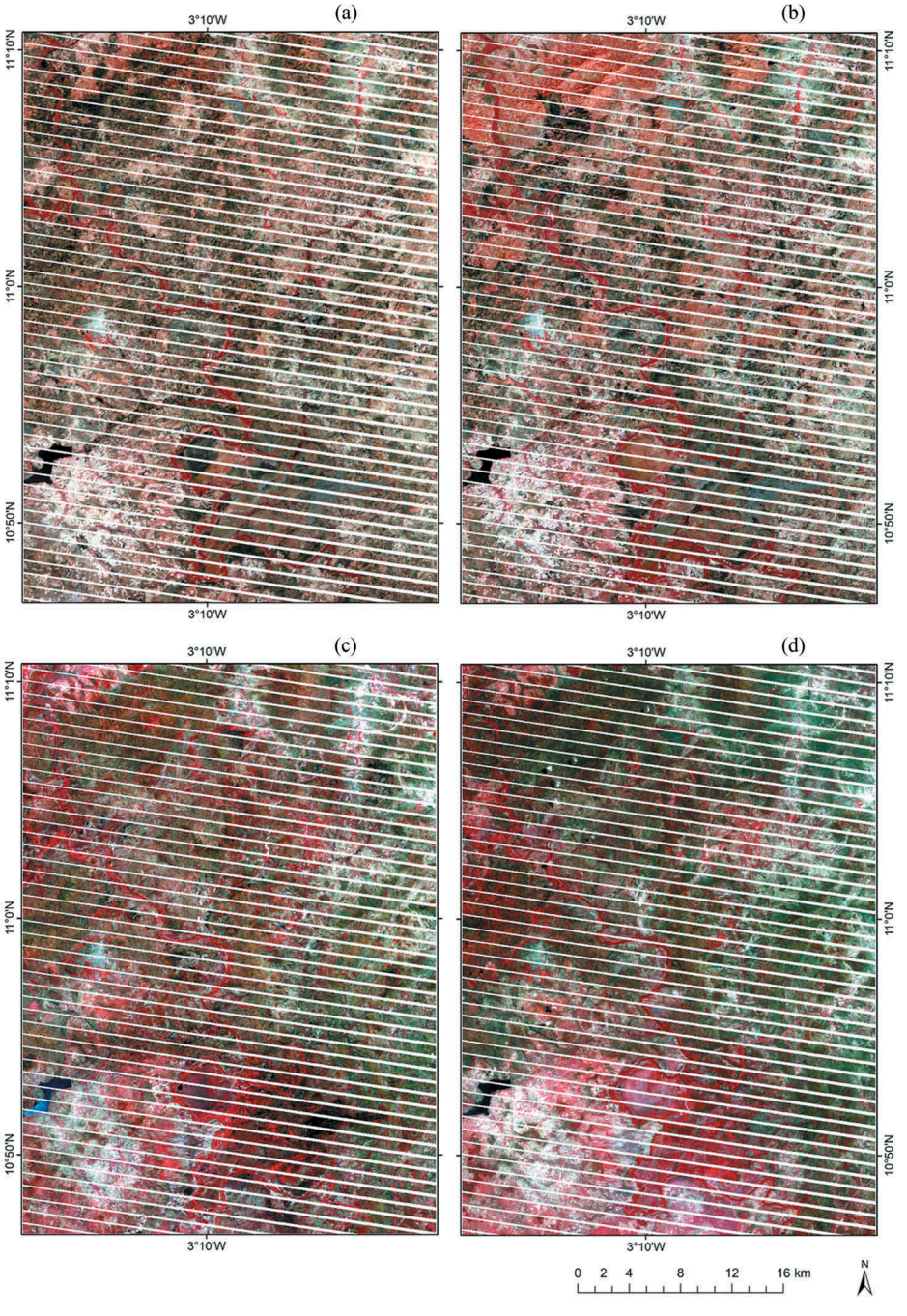

Figure 2. Landsat SLC-off images used for gap filling (band combination 4-3-2): (a & b) are the target and input images, respectively, for time step 1 (dry season); (c & d) are target and input images, respectively, for time step 2 (rainy season).

2.3.2. Localized linear histogram matching

The LLHM which was developed by a joint USGS/NASA (National Aeronautics and Space Administration) research team (USGS 2004; Desai and Ganatra 2012) and was the first gap-filling algorithm after the failure of the scan line corrector on board the Landsat 7 ETM+ sensor. In the LLHM method, the linear transformation is obtained by calculating the gain and bias using the mean and standard deviation within a localized moving window around each pixel in the SLC-on or another SLC-off image to obtain the localized linear transform function. Then, it transforms the pixel value to fill the missing data pixels in the target SLC-off image (Suliman 2016; Sadiq et al. 2014). All valid data within the target image are retained. Two or more fill scenes may be used due to the geometry of the gaps. In many instances, the gaps in the target and input images will overlap, resulting in some left-over gaps in the target image. In such an instance, more than one fill images should be used before the gaps can be completely filled. The detailed methodology of LLHM algorithm has been outlined on the USGS website (USGS 2004) and the IDL compiled version for ENVI (Environment for Visualizing Images) is online (YCEO 2013).

2.3.3. Neighbourhood similar pixel interpolator

The NSPI which was proposed by Chen et al. (2011) is based on the assumption that neighbouring pixels which are close to SLC-off gaps share common spectral characteristics and temporal patterns of changes with the missing data pixels, if they are all of the same land use or cover type. In this case, it is necessary to search for similar pixels near the gaps. All the pixels in a similar class of an area are counted and their distance, similarity, and temporal measures are calculated before a new radiometric value is predicted for the missing pixel value. The steps included in the NSPI are (i) selection of neighbouring similar pixels, (ii) calculation of the weights for similar pixels, (iii) calculation of the target pixel value, and (iv) data quality flag generation. The NSPI can be applied to either TOA radiance or Digital Numbers (DN) value (if the radiometric calibration formula is the same between input and target images) or to TOA reflectance or reflectance products after performing atmospheric correction on the image. The detailed explanation of this method can be found in Chen et al. (2011) and the IDL code is online (Zhu 2016b). The parameters used are as follows: sample size of the sample pixel is 20, the maximum window size is 8, the estimated number of classes is 5, range of minimum and maximum DN values of the image is [0, 1], and the block size is 500. These parameters were selected based on the recommendations made by Chen et al. (2011).

2.3.4. Geostatistical neighbourhood similar pixel interpolator

GNSPI is a geostatistical approach which combines deterministic interpolation and geostatistical principles (Zhu, Liu, and Chen 2012). The technique uses physical or empirical models to first remove the trend of data in the target image and then adopts ordinary Kriging to predict the residual (Yin et al. 2017). One or more additional image(s) is/are needed together with the target image in the gap-filling process. The algorithm involves a six-step process: data de-trending using empirical or physical models (steps 1 & 2); estimation of the semi-variogram of the residuals arising from the de-trending model (step 3); prediction of the residuals of the locations without observation from ordinary kriging (steps 4 & 5); final prediction of locations without observation is obtained by adding back the trend (step 6) (Zhu, Liu, and Chen 2012). The GNSPI code is written in Interactive

Data Language (IDL) and can be accessed online (Zhu 2016a). The following parameters were set based on the advice of the developers: sample size is 20, the maximum window size is 12, the estimated number of classes is 5, range of minimum and maximum DN values of the image is [0, 1], and the block size is 500 (Zhu, Liu, and Chen 2012).

2.4. Method

2.4.1. Gap-filling process and analysis

All four aforementioned data preparation routines and processes were utilized in order to produce the final gap-filled images for comparison. The WLR-LPRM algorithm was implemented using a packaged software that runs on windows operating system. The NSPI and GNSPI codes were implemented on the IDL platform in ENVI software whiles the LLHM algorithm was implemented using a packaged software which was installed and run on ENVI software as a toolbox. The gap-filled images were assessed in two ways: (i) based on the DNs of the resulting images, (ii) based on classification results. For the assessment based on the DN values, the mean and standard deviation of the filled areas were calculated and compared. In addition, the histograms of all the six bands for S1 were plotted for qualitative comparison. For the comparison based on the classification results, the balanced accuracy (BA) per class, the OA and κ obtained from the error matrices after classification were taken into account (Congalton 1991). It was assumed that since all the gap-filled images will be classified with the same algorithm, training and validation samples, this process can be used to explain the effectiveness of the filled images in a classification application (Zhu, Liu, and Chen 2012). This assumption provides a fair basis for comparing the OA and κ of each gap-filled image. Also, the filled results were visually checked to determine whether they were spatially continuous, and whether there were any anomalies in the filled image (Chen et al. 2011; Maxwell, Schmidt, and Storey 2007; Pringle, Schmidt, and Muir 2009). A comparison between the two time steps was done to ascertain whether they all had similar results.

2.4.2. Image classification using random forest

The resulting gap-filled images were classified into various LULC types using the 'superclass' command under RStoolbox package (Leutner 2017) in R stats. Random Forest (RF) is a supervised machine learning technique that is widely used by researchers in remote sensing (Forkuor et al. 2014; Kalbi, Fallah, and Shataee 2014; Stefanski et al. 2014; Watts et al. 2011; Meng et al. 2017). As a non-parametric decision-tree (DT) based classifier, RF combines the results of a given number of DTs. DT is a tree-like hierarchy, made up of a root node, which involves all samples, internal or split nodes with a decision rule, and final leave nodes, representing the different classes. Tree 'branches' are split by reducing the uncertainty present in the data and hence the probability of misclassification. Each tree in the forest is trained by a randomly selected subset of samples. The performance of an RF depends on the predicted accuracy of the individual trees and the correlation between the trees. In the classification process, each tree in the forest casts a unit vote for the most popular class (Breiman 2001). It also has an internal unbiased estimator of the training set error known as 'out-of-bag' (OOB) for cross validation-like accuracy measure. The advantages of RF compared to other classification algorithms include; (i) very high accuracy and robust results; (ii) a way of determining variable importance and (iii) ability

to model complex interactions among predictor variables (Cutler et al. 2007). The implementation of RF classification requires two parameters: the total number of trees to be constructed, in this study 500, and the number of variables to be randomly selected as candidates at each node split, here 1000.

2.4.3. Accuracy assessment

To evaluate the performance of the RF classifier, classification accuracies were determined using a set of independent data (validation data). The OA and κ are the most commonly used statistics for evaluating the overall performance of LULC classification (Congalton 1991). The OA is the proportion of pixels that are correctly classified, whereas κ measures the agreement between the classification by assessing if the confusion matrix is significantly different from a random result (Zijdenbos et al. 1994; Smits, Dellepiane, and Schowengerdt 1999; Congalton 1991). In comparing two classifications, higher OA and κ represent more accurate results from the overall prediction perspective (Kalbi, Fallah, and Shataee 2014; Stefanski et al. 2014). To determine the per class performance, the balanced accuracy (BA) per class, which can be defined as the arithmetic mean of sensitivity and specificity was calculated according to equations 1–3:

$$\mathrm{BA} = \frac{(\text{sensitivity} + \text{specificity})}{2} \tag{1}$$

The sensitivity (producer's accuracy or true positive rate) is the percentage of the pixels which were correctly classified. To calculate the specificity, the sensitivity is normalized by either the total number of observations predicted to the class or the actual number of observations in that class (Brodersen et al. 2010; Garcia, Mollineda, and Sanchez 2009; Sokolova, Japkowicz, and Szpakowicz 2006).

$$\text{Sensitivity} = \frac{\mathrm{TP}}{(\mathrm{TP} + \mathrm{FN})} \tag{2}$$

$$\text{Specificity} = \frac{\mathrm{TN}}{(\mathrm{FP} + \mathrm{TN})} \tag{3}$$

where TP is true positive, FN is false negative, TN is true negative, and FP is false positive rates. Note: TN for a class is the sum of the values in the leading diagonal except the value of that particular class.

The class BA utilizes three core elements from each class within the confusion matrix: the total number of correctly classified pixels, the total number of pixels predicted into that class, and the total number observed in the data. In this study, the ground truth data were split 70% to 30% for training and validation, respectively. The random seeds were set to the same values before training the RF model. This was done to ensure that the same random samples were used in each of the four algorithms and permit a direct comparison of their results (Forkuor et al. 2017a).

3. Results and discussion

3.1. Filled Landsat 7 ETM+ SLC-off image

Figure 3 shows the resulting Landsat 7 ETM+ SLC-off images for the two time steps displayed in a false colour composite (4-3-2). Although the gap-filling methods cannot perfectly restore an SLC-off image, the resultant images look excellent. No obvious visual differences were observed between the pixels of the filled areas and the other areas. Visually, all the filled images have no data gaps (stripes) left on them. They look spatially continuous with no anomalies and they all look similar. This implies that all the methods have comparable abilities for gap filling in a heterogeneous landscape of West Africa with cloud-free images. The results from the LLHM were visually good just like the results from the other methods although the other methods claim to be more robust than the LLHM (Romero-sanchez et al. 2015). The inclusion of the time-series images in the NSPI and GNSPI did not make any visual difference from the WRL-LPRM and LLHM which required no time-series image. This may be as a result of the non-over lapping nature of the gaps in the images used for this exercise and the fact that the time-series image was from the same season and temporally close to the target and input images.

Figure 4 shows two zoomed-in areas of the gap-filled images for S1 and further confirms the effectiveness of all the gap-filling methods. Panel 1 shows a dam (black colour) area with a major road along the retaining wall and large areas of croplands around the dam. Panel 2 shows a forest reserve (big red stripe) with a major road through

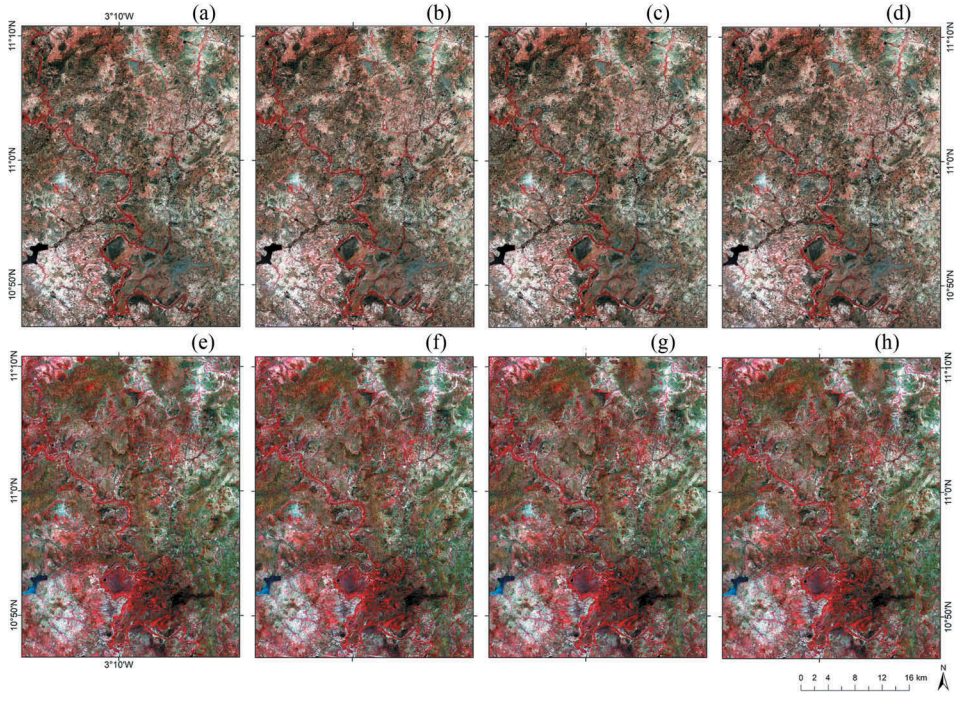

Figure 3. Results of gap-filled Landsat 7 ETM+ SLC-off images using the four methods (band combination 4-3-2). (a & e) WLR-LPRM; (b & f) LLHM; (c & g) NSPI; and (d & h) GNPSI. (a – d) represents time step 1, dry season. (e – f) represents time step 2, rainy season.

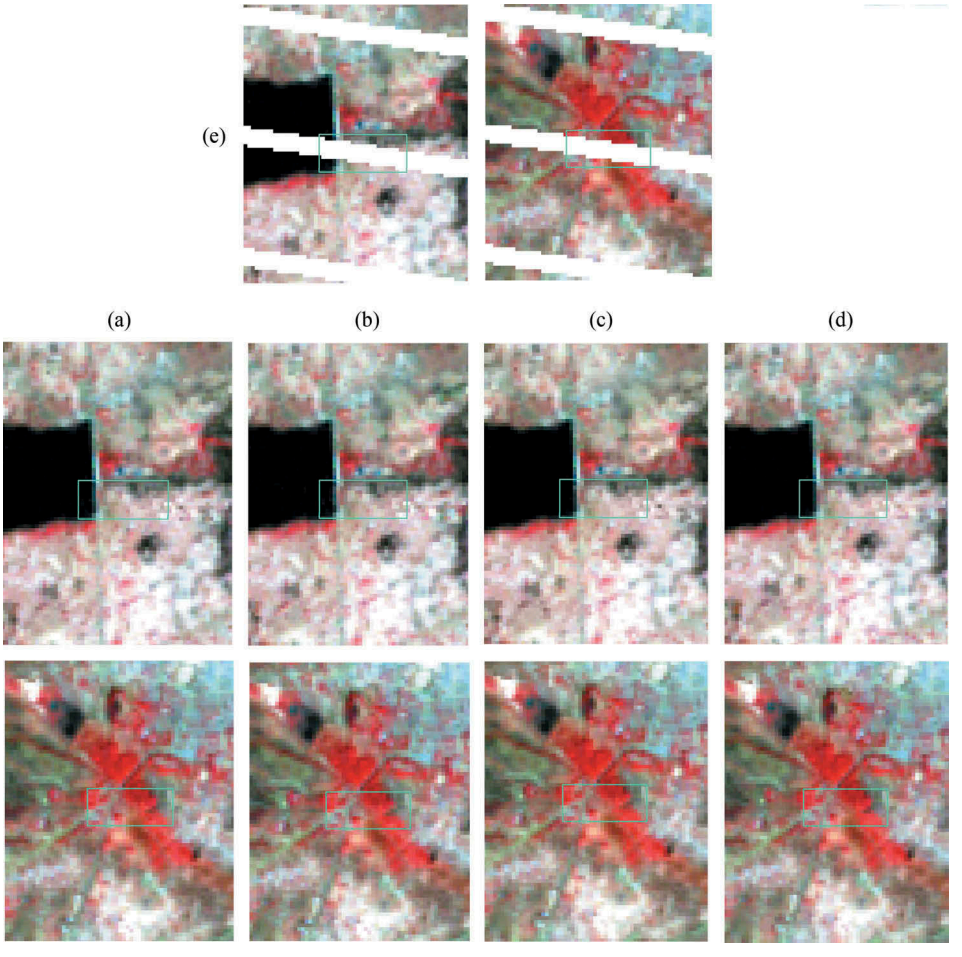

Figure 4. Zoomed areas of original SLC-off image and gap-filled images for S1 (band combination 4-3-2); columns: (a) WLR_LPRM; (b) LLHM; (c) NSPI; and (d) GNPSI methods; Row (e) is the original SLC-off image (the left image shows a dam (black) surrounded by croplands and the right image shows a forest reserve (red) area). The area of interest is within the green rectangle.

it. It is evident from Panels 1 and 2 that all the gaps in the original image (Figure 2) have completely been filled by all the four methods.

In addition to the visual comparison, the histograms of all the six bands of only the filled areas were generated and their mean and standard deviations calculated. From Figure 5 which shows the histograms for S1 (dry season), it can be observed that the pixel values show similar distributions for the filled areas using the four methods for all bands. Nonetheless, the LLHM gave a slightly different distribution for bands 1 and 4. Likewise, the means and standard deviations of the bands were similar in most cases. In the case of the LLHM, band 3 gave a slightly different mean value (μ of about 0.001 more than the others) (Table 2). For the WLR-LPRM, bands 5 and 7 also had means (B5: μ of about 0.003 less and B7: μ of about 0.004 less) which were slightly different from the other three methods. The results from S2 (rainy season) for the four methods had similar pixel value distributions, means, and standard deviations trend like S1 (Table 2), with

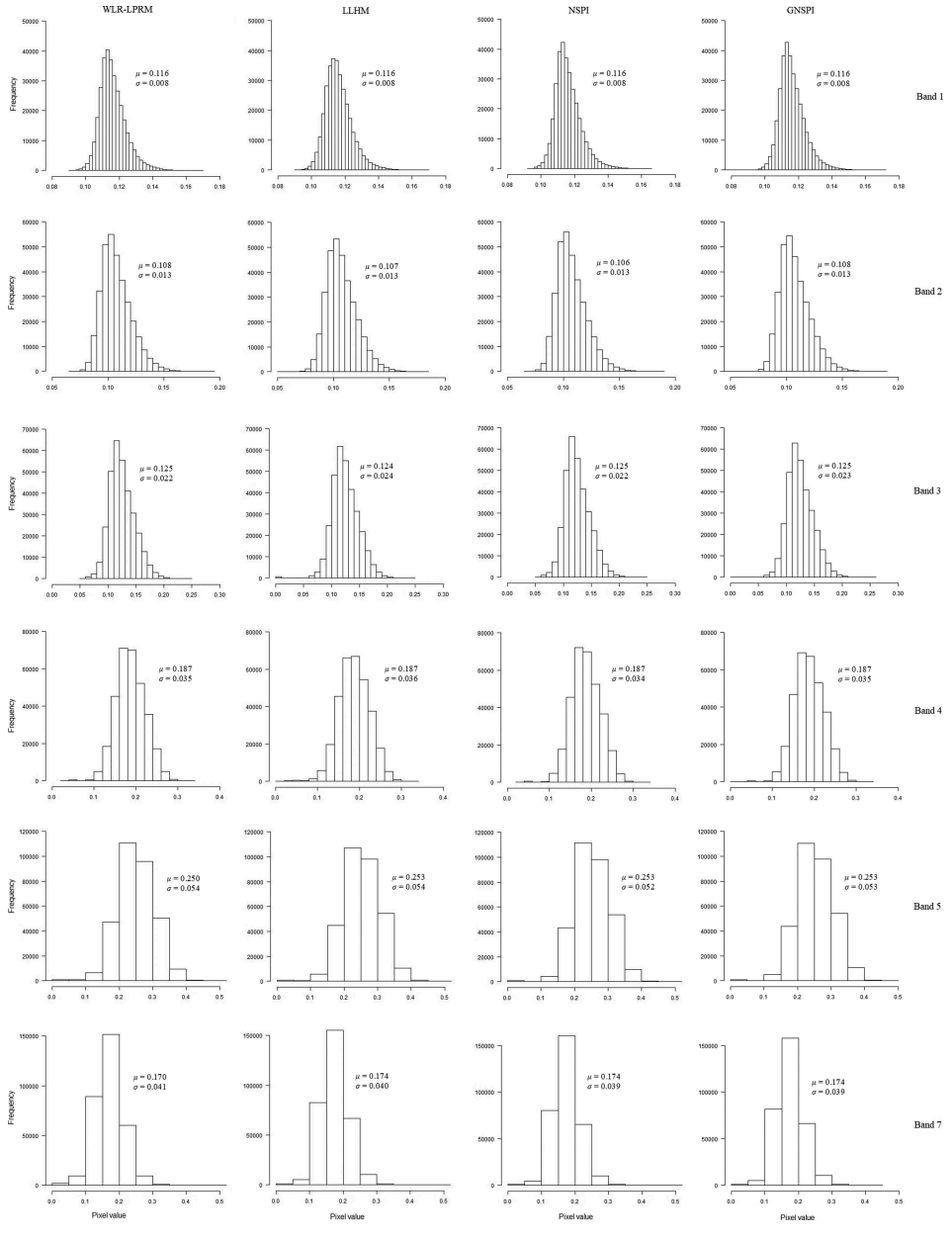

Figure 5. Histograms and statistic of bands for only the filled gaps using the four methods for S1 (dry season). The rows represent the spectral bands (Band 1–5 & 7). The columns represent the gap-filling methods (WLR-LPRM, LLHM, NSPI, and GNSPI).

WLR-LPRM having a slight deviation of mean for bands 5 and 7 (B5: μ of about 0.004 less and B7: μ of about 0.004 less). All the other bands gave similar mean values for all the four methods. A comparison of the trends of mean and standard deviation values for each of the bands for the different time steps shows a similar trend in most cases with very few deviations.

Table 2. Mean (μ) and standard deviation (σ) of band pixel values for only filled gaps using the four methods. S1 represents time step 1 (dry season) and S2 time step 2 (rainy season).

		WLR-LPRM		LLHM		NSPI		GNSPI	
Band	Statistic	S1	S2	S1	S2	S1	S2	S1	S2
B1	μ	0.116	0.122	0.116	0.122	0.116	0.122	0.116	0.122
	σ	0.008	0.007	0.008	0.008	0.008	0.007	0.008	0.007
B2	μ	0.108	0.119	0.107	0.119	0.106	0.119	0.108	0.119
	σ	0.013	0.011	0.013	0.011	0.013	0.011	0.013	0.011
B3	μ	0.125	0.132	0.124	0.132	0.125	0.132	0.125	0.132
	σ	0.022	0.018	0.024	0.019	0.022	0.018	0.023	0.018
B4	μ	0.187	0.206	0.187	0.207	0.187	0.206	0.187	0.206
	σ	0.035	0.021	0.036	0.023	0.034	0.021	0.035	0.021
B5	μ	0.250	0.260	0.253	0.264	0.253	0.264	0.253	0.264
	σ	0.054	0.035	0.054	0.037	0.052	0.036	0.053	0.036
B7	μ	0.170	0.163	0.174	0.167	0.174	0.167	0.174	0.167
	σ	0.041	0.033	0.040	0.032	0.039	0.031	0.039	0.031

3.2. Accuracy assessment from LULC classification

The summary of the results (OA and κ) obtained after the validation of the classification model is presented in Table 3.

For S1, it can be seen that GNSPI obtained the highest OA (97.1%) and κ (0.947) indicating that GNSPI is more robust than the other three methods. The WLR-LPRM outperformed the NSPI and LLHM with OA and κ values of 96.9% and 0.943, respectively, although the OA values were very close. In the works of Maxwell (2004) and Zeng, Shen, and Zhang (2013), the LLHM was rated as the least robust because it had worse results. The results from this research also proved the same. This notwithstanding, the LLHM did not perform badly at all although it had the least OA and κ. It was only 0.1 and 0.001 away from the NSPI for OA and, respectively. Although most of the pre-defined conditions (few clouds, low temporal variability, and minimal separation date) for the LLHM algorithm to achieve optimum results were met (Scaramuzza, Micijevic, and Chander 2004; Zhang, Li, and Travis 2007), it achieved the least performance. This can be attributed to the fact that the images were not checked for fire scars which is one of the pre-defined conditions and sun glint (Chen et al. 2011). Secondly, the simple nature of the algorithm can also contribute to its performance. In the case of LULC which has a huge anthropogenic effect especially in West Africa, assuming a linear relationship between the temporal variability of a LULC type may be misleading.

Table 3. Classification statistics of the gap-filled Landsat 7 ETM+ SLC-off images using WLR-LPRM, LLHM, NSPI, and GNSPI, for the two-time steps as shown in Figure 3. S1 and S2 are the results from the dry and rainy seasons, respectively.

	BA [%]							
	WLR-LPRM		LLHM		NSPI		GNSPI	
LULC	S1	S2	S1	S2	S1	S2	S1	S2
Bare land	98.3	81.5	98.3	83.6	95.8	81.4	98.4	81.6
Cropland	97.0	95.0	96.5	94.6	96.5	94.6	97.0	95.0
Settlement	97.8	90.7	97.9	82.4	96.5	87.9	97.9	90.9
Waterbody	99.5	99.2	99.5	99.2	99.5	99.2	99.5	99.2
Vegetation	99.4	94.1	95.9	92.6	96.9	91.6	97.4	92.8
OA (%)	**96.9**	**94.3**	**96.6**	**93.4**	**96.7**	**93.7**	**97.1**	**94.6**
Kappa ()	**0.943**	**0.895**	**0.938**	**0.878**	**0.939**	**0.882**	**0.947**	**0.899**

The comparison of the performance of the various LULC classes using the BA shows the strength of the GNSPI in the bare land class. For Cropland, the GNSPI and WLR-LPRM achieved comparable accuracies (BA of 97.0%). The GNSPI again had the same accuracy with the LLHM (BA of 97.9%) for settlement. All the four methods produced the same BA (99.5%) for Waterbody. In the vegetation class, the WLR-LPRM obtained the highest BA of 99.4%. The results show that the WLR-LPRM performed very well. Its slight shortfall can be attributed to its linear relationship assumption part which has a greater chance to be invalid in reality (Yin et al. 2017).

The difference in the season did not affect the performance rating of the gap-filling methods because the outcome of S2 had a similar trend like that of S1 (Table 3). The GNSPI obtained the highest OA of 94.6% and κ of 0.899. This was closely followed by the WLR-LPRM (OA of 94.3% and κ of 0.895). The NSPI followed with the LLHM obtaining the least values of OA and κ.

However, the BA showed some slight changes in the class accuracies. The LLHM had the highest accuracy (83.6%) in the bare land class. For Cropland, the GNSPI and WLR-LPRM achieved comparable accuracies (BA of 95%). The GNSPI was slightly ahead of the WLR-LPRM in the settlement class with the NSPI and LLHM following suite. Synonymous to the trend in S1, all the four methods produced the same BA (99.2%) for Waterbody. Finally, the WLR-LPRM outperformed (BA of 94.1%) the other three in the vegetation class.

The strength of the GNSPI in both time steps can be attributed to the fact that it applies a geostatistical approach which is influenced by the spatial dependence of the images. First, it utilizes the temporal information from the input images which is used to predict the values of all pixels outside the gaps. Secondly, GNSPI uses the sample pixels, which have high spectral similarity with the target pixels for predicting the values of the target pixels (Zhu, Liu, and Chen 2012). In the instance where there is no time-series image or second input image which is temporally closer to the target image, the WLR-LPRM can be an option to consider since its accuracies were relatively close to the GNSPI.

A comparison of classification accuracies between the two time steps revealed higher values of BA, OA and κ (Table 3) in S1. This can be attributed to the fact that in WA, most LULC types can better be distinguished at the early stages of the dry season than in the rainy season where most areas have turned green. This result is similar to a study conducted by Liu et al. (2015) in the study area. Figure 6 shows the classified gap-filled images using the four algorithms for S1 (dry season). The linear vegetation represents a riverine vegetation.

3.3. Implication for LULC mapping in West Africa

The results of this research give a very bright outlook for LULC mapping in a data-scarce region such as WA because

- there is a high possibility of correcting existing and future Landsat 7 ETM+ SLC-off images in West Africa for various LULC analyses.
- considering the high persistence of cloud cover in WA, the concurrent operation of Landsat 8 and Landsat 7 ETM+ will help to increase the number of Landsat images needed to build a time series once Landsat 7 ETM+ SLC-off images can be utilized after gap filling.

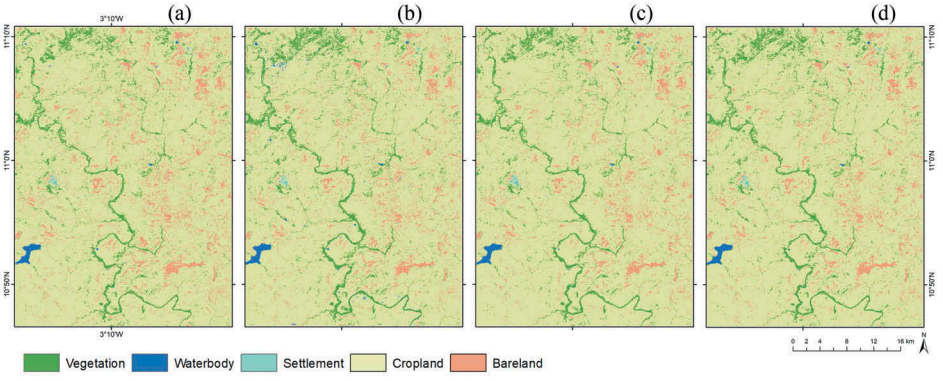

Figure 6. Classification results of gap-filled Landsat 7 ETM+ SLC-off images using the four methods for S1 (dry season); a, b, c, & d represent the classified image from WLR-LPRM, LLHM, NSPI, and GNPSI algorithms, respectively.

- there is hope for LULC applications which involve historical analysis that depends on the utilization of previous Landsat 7 ETM+ SLC-off images.
- once Landsat 7 ETM+ SLC-off images are gap filled, there will be a fairground for comparison with images from other Landsat sensors in LULC classification in multi-sensor applications.

4. Conclusion

Although the SLC on board the Landsat 7 ETM+ has failed to account for about 22% of the data lost from each scene, the remaining spectral information maintains the same radiometric and geometric quality as images collected prior to the failure (Storey et al. 2005). Therefore, the development of gap-filling methods to correct the no-data areas of the SLC-off images was very vital. Although some of the gap-filling methods have proven to be better than others, some researchers have identified their limitations (Romero-sanchez et al. 2015; Yin et al. 2017).

Visually, all the four gap-filling methods investigated in this study were able to completely fill the gaps in the Landsat 7 ETM+ SLC-off images for the two time steps. The resultant images show similar qualities with no artefacts. The histograms from each band for only the filled areas for all the four methods also gave similar distributions and this can be observed in their means and standard deviations, although the LLHM gave a slightly different distribution for bands 1 and 4. From the LULC classification, all the four gap-filling methods provided satisfactory results which are comparable to that of Zoungrana et al. (2015). This is evident in the OA of classification which is above 96% and 93% for the images for the dry and rainy seasons, respectively. This means that less than 4% of the pixels are classified as different LULC types in all instances for the dry season image and less than 7% in the rainy season image. Nevertheless, it cannot be overlooked that the GNSPI had the highest accuracy in both dry and rainy season's gap-filled images. In the instance where no time-series image is available, we recommend the WLR-LPRM since it gave very good results.

Overall, this research agrees with previous research by Zhu, Liu, and Chen (2012), Romero-sanchez et al. (2015) and Yin et al. (2017) on other continents with a totally different

landscape from that of West Africa but still the superiority of the GNSPI in different seasons was recorded over the other three methods.

Finally, the findings of this research are based on the use of a set of images (target, input, and time series) from the same season (dry and rainy seasons), temporally close and cloud free in a highly heterogeneous landscape. Future research must focus on testing the robustness of the algorithms for filling gaps in images with large differences in radiance (i.e. input and target). This knowledge will be useful in instances where temporally close images are not available due to, for example, excessive cloud cover.

Acknowledgements

My sincere appreciation goes to the Federal Ministry of Education and Research (BMBF) and West African Science Centre on Climate Change and Adapted Land Use (WASCAL) for providing the scholarship for my PhD research out of which comes this publication.

Disclosure statement

No potential conflict of interest was reported by the authors.

Funding

This work was supported by the Bundesministerium für Bildung und Forschung;

ORCID

Yaw Mensah Asare http://orcid.org/0000-0001-8275-4604

References

Aksoy, E., G. Özsoy, and M. S. Dirim. 2009. "Soil Mapping Approach in GIS Using Landsat Satellite Imagery and DEM Data." *African Journal of Agricultural Research* 4 (11): 1295–1302. http://www.academicjournals.org/AJAR

Azabdaftari, A., and F. Sunar. 2016. "Soil Salinity Mapping Using Multitemporal Landsat Data." *The International Archives of the Photogrammetry, Remote Sensing and Spatial Information Sciences* XLI: B7. doi:10.5194/isprsarchives-XLI-B7-3-2016.

Bhatti, S. S., and N. Kumar Tripathi. 2014. "Built-up Area Extraction Using Landsat 8 OLI Imagery." *GIScience & Remote Sensing* 51 (4): 445–467. doi:10.1080/15481603.2014.939539.

Breiman, L. 2001. "Random Forests." *Machine Learning* 45 (1): 5–32. doi:10.1023/A:1010933404324.

Brodersen, K. H., C. S. Ong, K. E. Stephan, and J. M. Buhmann. 2010. "The Balanced Accuracy and Its Posterior Distribution." In 20th *International Conference on Pattern Recognition (Istanbul)*, 3121–3124. IEEE. doi:10.1109/ICPR.2010.764.

Callo-Concha, D., T. Gaiser, and F. Ewert. 2012. "Farming and Cropping Systems in the West African Sudanian Savanna." 100. Working Paper. Bonn. Accessed 16 July 2018. http://hdl.handle.net/10419/88290

Chen, J., X. Zhu, J. E. Vogelmann, F. Gao, and S. Jin. 2011. "A Simple and Effective Method for Filling Gaps in Landsat ETM + SLC-off Images." *Remote Sensing of Environment* 115 (4): 1053–1064. Elsevier B.V. doi:10.1016/j.rse.2010.12.010.

Congalton, R. G. 1991. "A Review of Assessing the Accuracy of Classifications of Remotely Sensed Data." *Remote Sensing of Environment* 37 (1): 35–46. doi:10.1016/0034-4257(91)90048-B.

Cutler, D. R., T. C. Edwards, K. H. Beard, A. Cutler, K. T. Hess, J. Gibson, and J. J. Lawler. 2007. "Random Forests for Classification in Ecology." *Ecology* 88 (11): 2783–2792. doi:10.1890/07-0539.1.

Desai, M., and A. Ganatra. 2012. "Survey on Gap Filling in Satellite Images and Inpainting Algorithm." *International Journal of Computer Theory and Engineering* 4 (3): 341–345. doi:10.7763/IJCTE.2012.V4.479.

Esch, T., V. Himmler, G. Schorcht, M. Thiel, T. Wehrmann, F. Bachofer, C. Conrad, M. Schmidt, and S. Dech. 2009. "Large-Area Assessment of Impervious Surface Based on Integrated Analysis of Single-Date Landsat-7 Images and Geospatial Vector Data." *Remote Sensing of Environment* 113: 1678–1690. doi:10.1016/j.rse.2009.03.012.

FAO. 2000. "Land Cover Classification System (LCCS): Classification Concepts and User Manual." http://www.fao.org/docrep/003/x0596e/x0596e00.htm

Forkuor, G., C. Conrad, M. Thiel, T. Ullmann, and E. Zoungrana. 2014. "Integration of Optical and Synthetic Aperture Radar Imagery for Improving Crop Mapping in Northwestern Benin, West Africa." *Remote Sensing* 6 (7): 6472–6499. doi:10.3390/rs6076472.

Forkuor, G., K. Dimobe, I. Serme, and E. J. Tondoh. 2017a. "Landsat-8 Vs. Sentinel-2 : Examining the Added Value of Sentinel-2 ' S Red-Edge Bands to Land-Use and Land-Cover Mapping in Burkina Faso." *GIScience & Remote Sensing*: 1–24. Taylor & Francis. doi:10.1080/15481603.2017.1370169.

Forkuor, G., O. K. L. Hounkpatin, G. Welp, and M. Thiel. 2017b. "High Resolution Mapping of Soil Properties Using Remote Sensing Variables in South- Western Burkina Faso : A Comparison of Machine Learning and Multiple Linear Regression Models." *PLoS ONE* 12 (1): e0170478. doi:10.1371/journal.pone.0170478.

Garcia, V., R. A. Mollineda, and J. S. Sanchez. 2009. "Index of Balanced Accuracy : A Performance Measure for Skewed Class Distributions." In *IbPRIA 2009*, edited by H. Araujo et al., LNCS 5524. 441–448. Springer-Verlag Berlin, Heidelberg. doi:10.1007/978-3-642-02172-5_57.

Ghansah, B., Y. M. Asare, E. T. Tchao, and E. K. Forkuo. 2016. "Mapping the Spatial Changes in Lake Volta Using Multitemporal Remote Sensing Approach." *Lakes and Reservoirs: Research and Management* 21: 206–215. doi:10.1111/lre.12138.

Hamuda, E., B. M. Ginley, M. Glavin, and E. Jones. 2018. "Improved Image Processing-Based Crop Detection Using Kalman Filtering and the Hungarian Algorithm." *Computers and Electronics in Agriculture* 148: 37–44. doi:10.1016/j.compag.2018.02.027.

Hellweger, F. L., P. Schlosser, U. Lall, and J. K. Weissel. 2004. "Use of Satellite Imagery for Water Quality Studies in New York Harbor." *Estuarine, Coastal and Shelf Science* 61: 437–448. doi:10.1016/j.ecss.2004.06.019.

Hipt, O. D. F., B. Diekkrüger, G. Steup, Y. Yira, T. Hoffmann, and M. Rode. 2017. "Applying SHETRAN in a Tropical West African Catchment (Dano, Burkina Faso)—Calibration, Validation, Uncertainty Assessment." *Water* 9: 101. doi:10.3390/w9020101.

Hu, T., J. Yang, X. Li, and P. Gong. 2016. "Mapping Urban Land Use by Using Landsat Images and Open Social Data." *Remote Sensing* 8: 151. doi:10.3390/rs8020151.

International Union of Soil Sciences (IUSS) working group. 2006. "World Reference Base for Soil Resources 2006. 2nd Ed." Rome, Italy. Accessed 15 February 2018. http://www.fao.org/3/a-a0510e.pdf

Jarman, M. L., N. G. Jarman, and D. Edwards. 1983. "Remote Sensing and Vegetation Mapping in South Africa." *Bothalia* 14 (2): 271–282. doi:10.4102/abc.v14i2.1172.

Kalbi, S., A. Fallah, and S. Shataee. 2014. "Forest Stand Types Classification Using Tree-Based Algorithms and SPOT-HRG Data." *International Journal of Environmental Resources Research* 2 (1): 263–278. doi:10.22069/ijerr.2014.1677.

Kleemann, J., G. Baysal, H. N. N. Bulley, and C. Fürst. 2017. "Assessing Driving Forces of Land Use and Land Cover Change by a Mixed-Method Approach in North-Eastern Ghana, West Africa." *Journal of Environmental Management* 196: 411–442. doi:10.1016/j.jenvman.2017.01.053.

Laili, N., F. Arafah, L. M. Jaelani, L. Subehi, A. Pamungkas, E. S. Koenhardono, and A. Sulisetyono. 2015. "Development of Water Quality Parameter Retrieval Algorithms for Estimating Total Suspended Solids and Chlorophyll-A Concentration Using Landsat-8 Imagery at Poteran Island Water." *ISPRS Annals of the Photogrammetry, Remote Sensing and Spatial Information Sciences* II (2/W2). doi:10.5194/isprsannals-II-2-W2-55-2015.

Laurin, G. V., V. Liesenberg, Q. Chen, L. Guerrieroa, F. Del Frate, A. Bartolini, D. Coomes, B. Wileborec, J. Lindsell, and R. Valentini. 2012. "Optical and SAR Sensor Synergies for Forest and Land Cover Mapping in a Tropical Site in West Africa." *International Journal of Applied Earth Observation and Geoinformation* 21: 7–16. doi:10.1016/j.jag.2012.08.002.

Leslie, C. R., L. O. Serbina, and H. M. Miller. 2017. "Landsat and Agriculture — Case Studies on the Uses and Benefits of Landsat Imagery in Agricultural Monitoring and Production." *Virginia*. doi:10.3133/ofr20171034.

Leutner, B. 2017. "Tools for Remote Sensing Data Analysis 'RStoolbox'." CRAN. Accessed 20 January 2018. http://bleutner.github.io/RStoolbox

Liu, J., J. Heiskanen, E. Aynekulu, and P. K. E. Pellikka. 2015. "Seasonal Variation of Land Cover Classification Accuracy of Landsat 8 Images in Burkina Faso." *The International Archives of the Photogrammetry, Remote Sensing and Spatial Information Sciences* XL (7/W3): 455–460. doi:10.5194/isprsarchives-XL-7-W3-455-2015.

Loveland, T. R., and J. L. Dwyer. 2012. "Landsat : Building a Strong Future. Remote Sens Environ Landsat : Building a Strong Future." *Remote Sensing of Environment* 122: 22–29. Elsevier B.V. doi:10.1016/j.rse.2011.09.022.

Lunetta, R. S., J. F. Knight, J. Ediriwickrema, J. G. Lyon, and L. Dorsey. 2006. "Land-Cover Change Detection Using Multi-Temporal MODIS NDVI Data Land-Cover Change Detection Using Multi-Temporal." *Environmental Protection* 43 (1): 142–154. doi:10.16/j.rse.2006.06.018.

Maxwell, S. K. 2004. "Filling Landsat ETM+ SLC-off Gaps Using a Segmentation Model Approach." *Photogrammetric Engineering & Remote Sensing* 1109–1111. http://www.ecognition.com/sites/default/files/305_pershighlight.pdf

Maxwell, S. K., G. L. Schmidt, and J. C. Storey. 2007. "A Multi - Scale Segmentation Approach to Filling Gaps in Landsat ETM + SLC - off Images." *International Journal of Remote Sensing* 28 (33): 5339–5356. doi:10.1080/01431160601034902.

Meng, R., J. Wu, K. L. Schwager, F. Zhao, P. E. Dennison, B. D. Cook, K. Brewster, T. M. Green, and S. P. Serbin. 2017. "Using High Spatial Resolution Satellite Imagery to Map Forest Burn Severity across Spatial Scales in a Pine Barrens Ecosystem." *Remote Sensing of Environment* 191: 95–109. Elsevier Inc. doi:10.1016/j.rse.2017.01.016.

Nawar, S., H. Buddenbaum, J. Hill, and J. Kozak. 2014. "Modeling and Mapping of Soil Salinity with Reflectance Spectroscopy and Landsat Data Using Two Quantitative Methods (PLSR and MARS)." *Remote Sensing* 6: 10813–10834. doi:10.3390/rs61110813.

Nyamugama, A., and V. Kakembo. 2015. "Monitoring Land Cover Changes and Fragmentation Dynamics in the Subtropical Thicket of the Eastern Cape Province, South Africa." *South African Journal of Geomatics* 4 (4): 397–413. doi:10.4314/sajg.v4i4.4.

Obahoundje, S., A. Diedhiou, E. A. Ofosu, S. Anquetin, B. François, J. Adounkpe, and Y. M. Kouame. 2018. "Assessment of Spatio-Temporal Changes of Land Use and Land Cover over South-Western African Basins and Their Relations with Variations of Discharges." *Hydrology* 5: 56. doi:10.3390/hydrology5040056.

Onojeghuo, A. O., and A. R. Onojeghuo. 2015. "Mapping Forest Transition Trends in Okomu Reserve Using Landsat and UK-DMC-2 Satellite Data." *South African Journal of Geomatics* 4 (4): 486–501. doi:10.4314/sajg.v4i4.9.

Pringle, M. J., M. Schmidt, and J. S. Muir. 2009. "Geostatistical Interpolation of SLC-off Landsat ETM+ Images." *ISPRS Journal of Photogrammetry and Remote Sensing* 64 (6): 654–664. doi:10.1016/j.isprsjprs.2009.06.001.

Romero-sanchez, M. E., R. Ponce-Hernandez, S. E. Franklin, and C. A. Aguirre-Salado. 2015. "Comparison of Data Gap-Filling Methods for Landsat ETM + SLC-off Imagery for Monitoring Forest Degradation in a Semi-Deciduous Tropical Forest in Mexico." *International Journal of Remote Sensing* 36 (11): 2786–2799. Taylor & Francis. doi:10.1080/01431161.2015.1047991.

Sadiq, A., A. Jabar, G. Sulong, and L. E. George. 2014. "Survey on Gap Filling Algorithms in Landsat 7 ETM + Images." *Journal of Theoretical and Applied Information Technology* 63 (1). http://www.jatit.org/volumes/Vol63No1/16Vol63No1.pdf

Scaramuzza, P., E. Micijevic, and G. Chander. 2004. "SLC Gap-Filled Products Phase One Methodology." http://landsat.usgs.gov/documents/SLC_Gap_Fill_Methodology.pdf

Shen, H. 2014. "Weighted Linear Regression (WLR) Open Source Code."Accessed 8 September 2017. http://sres.whu.edu.cn/shenhf/

Smits, P. C., S. G. Dellepiane, and R. A. Schowengerdt. 1999. "quality assessment of image classification algorithms for land-cover mapping: A review and A proposal for A cost-based approach." *International Journal of Remote Sensing* 20 (8): 1461–1486. doi:10.1080/014311699212560.

Sokolova, M., N. Japkowicz, and S. Szpakowicz. 2006. "Beyond Accuracy, F-Score and ROC: A Family of Discriminant Measures for Performance Evaluation." In *AI 2006: Advances in Artificial Intelligence*, edited by A. Sattar and B.-H. Kang, 1015–1021. Springer-Verlag Berlin, Heidelberg. doi: 10.1007/11941439_114.

Stefanski, J., T. Kuemmerle, O. Chaskovskyy, P. Griffiths, V. Havryluk, J. Knorn, N. Korol, A. Sieber, and B. Waske. 2014. "Mapping Land Management Regimes in Western Ukraine Using Optical and SAR Data." *Remote Sensing* 6: 5279–5305. doi:10.3390/rs6065279.

Storey, J., P. Scaramuzza, G. Schmidt, and J. Barsi. 2005. "Landsat 7 Scan Line Corrector-Off Gap-Filled Product Development Process." *In Proceedings of Pecora* 16: 23–27. http://www.asprs.org/a/publications/proceedings/pecora16/Storey_J.pdf

Suliman, S. I. 2016. "Locally Linear Manifold Model for Gap-Filling Algorithms of Hyperspectral Imagery: Proposed Algorithms and a Comparative Study." Michigan State University. Accessed 28 September 2018. https://search.proquest.com/10100699

USGS. 2004. "SLC-off Gap-Filled Products Gap-Fill Algorithm Methodology." doi:10.1017/CBO9781107415324.004.

USGS. 2013. "Landsat — A Global Land-Imaging Mission." *U.S. Geological Survey Fact Sheet*, Accessed 26 September 2017. https://pubs.usgs.gov/fs/2012/3072/fs2012-3072.pdf

Vittek, M., A. Brink, F. Donnay, D. Simonetti, and B. Desclé. 2014. "Land Cover Change Monitoring Using Landsat MSS/TM Satellite Image Data over West Africa between 1975 and 1990." *Remote Sensing* 6: 658–676. doi:10.3390/rs6010658.

Watts, J. D., S. L. Powell, R. L. Lawrence, and T. Hilker. 2011. "Improved Classification of Conservation Tillage Adoption Using High Temporal and Synthetic Satellite Imagery." *Remote Sensing of Environment* 115 (1): 66–75. Elsevier Inc. doi:10.1016/j.rse.2010.08.005.

White, J. C., M. A. Wulder, T. Hermosilla, N. C. Coops, and G. W. Hobart. 2017. "A Nationwide Annual Characterization of 25 Years of Forest Disturbance and Recovery for Canada Using Landsat Time Series." *Remote Sensing of Environment* 194: 303–321. doi:10.1016/j.rse.2017.03.035.

Wijedasa, L. S., S. Sloan, D. G. Michelakis, and G. R. Clements. 2012. "Overcoming Limitations with Landsat Imagery for Mapping of Peat Swamp Forests in Sundaland." *Remote Sensing* 4 (9): 2595–2618. doi:10.3390/rs4092595.

Williams, D. L., S. Goward, and T. Arvidson. 2006. "Landsat : Yesterday, Today, and Tomorrow." *Photogrammetric Engineering & Remote Sensing* 72 (10): 1171–1178. doi:10.14358/PERS.72.10.1171.

Wulder, M. A., S. M. Ortlepp, J. C. White, and S. Maxwell. 2008. "Evaluation of Landsat-7 SLC-off Image Products for Forest Change Detection." *Canadian Journal of Remote Sensing* 34 (2): 93–99. doi:10.5589/m08-020.

Yale Centre for Earth Observation (YCEO). 2013. "Landsat Gapfill IDL Model." YCEO. Accessed 9 February 2018. https://docs.google.com/file/d/0B3e_wo8OTO47b3c4ZHNyV0NmUkk/edit?pli=1

Yin, G., G. Mariethoz, and M. F. McCabe. 2016. "Gap-Filling of Landsat 7 Imagery Using the Direct Sampling Method." *Remote Sensing* 9 (1): 12. doi:10.3390/rs9010012.

Yin, G., G. Mariethoz, Y. Sun, and M. F. Mccabe. 2017. "A Comparison of Gap-Filling Approaches for Landsat-7 Satellite Data." *International Journal of Remote Sensing* 38 (23): 6653–6679. doi:10.1080/01431161.2017.1363432.

Zeng, C., H. Shen, and L. Zhang. 2013. "Recovering Missing Pixels for Landsat ETM + SLC-off Imagery Using Multi-Temporal Regression Analysis and a Regularization Method." *Remote Sensing of Environment* 131: 182–194. doi:10.1016/j.rse.2012.12.012.

Zhang, C., W. Li, and D. Civco. 2014. "Application of Geographically Weighted Regression to Fill Gaps in SLC-off Landsat ETM + Satellite Imagery." *International Journal of Remote Sensing* 35 (22): 7650–7672. Taylor & Francis. doi:10.1080/01431161.2014.975377.

Zhang, C., W. Li, and D. Travis. 2007. "Gaps - Fill of SLC - off Landsat ETM + Satellite Image Using a Geostatistical Approach." *International Journal of Remote Sensing* 28 (22): 5103–5122. doi:10.1080/01431160701250416.

Zhu, X. 2016a. "Neighbourhood Similar Pixel Interpolator (NSPI) IDL Code." https://sites.google.com/site/xiaolinzhurs/

Zhu, X. 2016b. "Geostatistical Neighbourhood Similar Pixel Interpolator (GNSPI) IDL Code." https://sites.google.com/site/xiaolinzhurs/

Zhu, X., D. Liu, and J. Chen. 2012. "A New Geostatistical Approach for Filling Gaps in Landsat ETM+ SLC-off Images." *Remote Sensing of Environment* 124: 49–60. Elsevier Inc. doi:10.1016/j.rse.2012.04.019.

Zijdenbos, A. P., B. M. Dawant, R. A. Margolin, and A. C. Palmer. 1994. "Morphometric Analysis of White Matter Lesions in MR Images: Method and Validation." *IEEE Transactions on Medical Imaging* 13 (4): 716–724. doi:10.1109/42.363096.

Zoungrana, B., C. Conrad, L. Amekudzi, M. Thiel, E. Da, G. Forkuor, and F. Löw. 2015. "Multi-Temporal Landsat Images and Ancillary Data for Land Use/Cover Change (LULCC) Detection in the Southwest of Burkina Faso, West Africa." *Remote Sensing* 7 (9): 12076–12102. doi:10.3390/rs70912076.